Chemical Engineering Journal 221 (2013) 25–31

Contents lists available at SciVerse ScienceDirect

Chemical Engineering Journal

journal homepage: www.elsevier.com/locate/cej

Methane reforming with carbon dioxide over mesoporous nickel–alumina composite catalyst

Kai Tao [a,*], Lei Shi [b], Qingxiang Ma [b], Ding wang [b], Chunyang Zeng [b], Chunlong Kong [a], Mingbo Wu [c], Liang Chen [a], Shenghu Zhou [a], Yibo Hu [a], Noritatsu Tsubaki [b,d,*]

[a] Ningbo Institute of Materials Technology and Engineering, Chinese Academy of Sciences, Ningbo, Zhejiang 315201, China
[b] Department of Applied Chemistry, School of Engineering, University of Toyama, Gofuku 3190, Toyama 930-8555, Japan
[c] State Key Laboratory of Heavy Oil Processing, China University of Petroleum, Qingdao 266555, China
[d] JST, ACT-C, Tokyo 102-8666, Japan

HIGHLIGHTS

- A mesoporous NiMA catalyst was prepared by one-pot EISA method.
- Prepared catalyst shows small Ni particle size and strong Ni-support interaction.
- The catalyst exhibits good catalytic performance for CO_2 reforming of CH_4.
- Carbon deposition is greatly suppressed over this catalyst.

ARTICLE INFO

Article history:
Received 27 September 2012
Received in revised form 21 January 2013
Accepted 23 January 2013
Available online 7 February 2013

Keywords:
Mesoporous
Nickel catalyst
Methane dry reforming
Al_2O_3

ABSTRACT

A mesoporous nickel–alumina composite catalyst prepared by one-pot evaporation-induced self-assembly (EISA) method, and a nickel supported EISA synthesized alumina catalyst prepared by impregnation method, were comparably studied for carbon dioxide reforming of methane reaction. The catalysts were characterized by N_2 physical adsorption, XRD, TPR, TEM, H_2 chemisorption and TG techniques. Although both mesoporous catalysts were active and stable for CO_2 reforming of CH_4, one-pot EISA synthesized catalyst showed superior catalytic performance to that prepared by impregnation method. It could be attributed to the higher nickel dispersion and stronger metal to support interaction of one-pot EISA synthesized catalyst, since small nickel crystalline size could retard coking and strong metal to support interaction could resist sintering.

1. Introduction

Methane reforming with carbon dioxide to produce syngas, which is also called dry reforming, has recently attracted much research attention. The syngas produced by this reaction has a low H_2/CO (<1) ratio, which can be converted to hydrocarbons and oxygenate compounds through Fischer–Tropsch synthesis (FTS) [1]. This reaction is also of great importance in the respect of global warming control, since two major greenhouse gases are transformed to valuable reactants ($CO + H_2$). However, there is still no large-scale application of CO_2 reforming of CH_4, due to the lack of efficient and stable catalysts [2]. Therefore, great efforts have been focused on development of excellent reforming catalysts using both noble and non-noble transition metals.

Noble metal catalyst, such as Rh [3], Ru and Pt [4–6], exhibited outstanding catalytic performance for methane dry reforming. However, due to the high price and limited availability of noble metal, their applications in industrial level is restricted. Alternatively, nickel-based catalysts with compatible activity and low cost have been extensively studied for methane dry reforming. However, the main drawback of Ni-based catalyst is the rapid deactivation of catalyst caused by coke formation and/or sintering of nickel under harsh reaction conditions [7,8]. Therefore, it is preferred to develop Ni catalyst with high coke resistance and stability for CO_2 reforming CH_4. α-Al_2O_3 and γ-Al_2O_3 are the most popular supports for reforming catalyst, because they are thermally stable and commercially available. But Ni–Al_2O_3 catalyst tends to coking. Many efforts have been done to suppress carbon deposition and to improve the catalyst stability. It is reported that highly dispersed Ni catalyst show good coke resistance, because the

* Corresponding authors. Address: Department of Applied Chemistry, School of Engineering, University of Toyama, Gofuku 3190, Toyama 930-8555, Japan. Tel./fax: +81 76 445 6846 (N. Tsubaki), tel.: +86 574 86685023; fax: +86 574 86685043 (K. Tao).
E-mail addresses: taokai@nimte.ac.cn (K. Tao), tsubaki@eng.u-toyama.ac.jp (N. Tsubaki).

1385-8947/$ - see front matter © 2013 Elsevier B.V. All rights reserved.
http://dx.doi.org/10.1016/j.cej.2013.01.073

ensemble size necessary for carbon formation is larger than that of for CH_4 reforming [9–11]. Strong interaction between Ni and support, such as TiO_2 or MgO is also beneficial for high activity and stability of the catalyst [12,13]. Another alternative way to improve stability of catalyst is addition of alkaline and alkaline earth metal promoters [14–16].

Mesoporous metal oxide with uniform pores, high surface, and narrow pore size distribution is highly desirable for catalysis applications. Recently, a mesoporous Ni–Al composite oxide was prepared by an EISA method developed by Morris et al. [17]. Compared with conventional single-step surfactant-templating method, $NiO–Al_2O_3$ with ordered mesopores could be obtained by self-assembly of the $(EO)_{20}(PO)_{70}(EO)_{20}$ triblock copolymer and metal precursors in ethanolic solution in the presence of nitric acid during the slow evaporation process. The EISA synthesized $NiO–Al_2O_3$ has high surface area and is thermally stable. Therefore, in this work, a mesoporous $NiO–Al_2O_3$ was prepared with similar method and applied in methane dry reforming. For comparison, a nickel catalyst supported on mesoporous alumina was also prepared by an impreganation method. The effect of preparation method on physicochemical properties and corresponding catalytic performance of nickel–alumina catalyst was investigated. It is expected that the well dispersed Ni species and high thermal stability of mesoporous $NiO–Al_2O_3$ will be beneficial for CO_2 reforming of CH_4.

2. Experimental

2.1. Catalyst preparation

A mesoporous nickel–alumina catalyst was prepared by an EISA method, according to the similar method reported in literature [17]. Typically, an appropriate amount of surfactant (Pluronic P123, PEO20-PPO70-PEO20, Adrich) was dissolved in ethanol under constant stirring. Then, nickel nitrate hexahydrate and aluminium isopropoxide were added in the solution. Once dissolved, the solution was furthered stirred at room temperature for 4 h. After that, solvent was evaporated for 48 h at 60 °C to develop a dry gel. The gel was calcined at 700 °C for 4 h with a temperature ramp of 1 °C/min. The mesoporous nickel–alumina catalyst was denoted as NiMA.

A mesoporous alumina (denoted as MA) was also prepared by the same EISA method as above without adding nickel precursor. Nickel impregnated MA catalyst (denoted as NiMA) was synthesized via incipient-wetness impregnation using $Ni(NO_3)_2{\cdot}6H_2O$ as a nickel precursor. The impregnated sample was dried at 120 °C overnight, followed by calcining at 700 °C for 4 h with a temperature ramp of 1 °C/min. Nickel loading was fixed at 5 wt% in both NiMA and Ni/MA catalysts.

2.2. Catalytic performance evaluation

Catalytic performance of the synthesized catalyst for methane dry reforming was evaluated in a fixed-bed quartz reactor (i.d. 9.4 mm) under atmospheric pressure. In each test, 0.1 g catalyst was loaded and in situ reduced at 750 °C for 2 h using a 5 vol% H_2/N_2 (50 ml/min) stream. A mixture containing CH_4, CO_2 and Ar ($CH_4/CO_2/Ar$ = 47.5/43.9/8.6) was used as reaction feed gas, in which argon was employed as the internal standard. W/F was fixed at 0.25 g-cat h mol^{-1}. An ice trap was set between the reactor and the gas chromatograph (GC) to remove the water from the effluent stream. Effluent CH_4, CO_2 and Ar were analyzed by a GC (Shimadzu GC 8A) with a Porapak Q column and a thermal conductivity detector (TCD); H_2 was analyzed by another GC (GC 320, GL Science) with an activated carbon column and a TCD.

The conversions of methane, carbon dioxide and H_2/CO ratio were calculated as follows:

$$CH_4 \text{ conversion, vol}\% = \frac{(CH_4/Ar)_{in} - (CH_4/Ar)_{out}}{(CH_4/Ar)_{in}} \times 100 \quad (1)$$

$$CO_2 \text{ conversion, vol}\% = \frac{(CO_2/Ar)_{in} - (CO_2/Ar)_{out}}{(CO_2/Ar)_{in}} \times 100 \quad (2)$$

$$H_2/CO \text{ ratio} = \frac{H_2 \text{ generation rate}}{CO \text{ generation rate}} \quad (3)$$

2.3. Catalyst characterization

X-ray diffraction (XRD) measurements of calcined catalyst and spent catalyst were performed using a Rigaku RINT2000 diffractometer with Cu Kα radiation in the range of 2θ angles 20–80°. Ni crystalline average size was calculated by $L = K\lambda/\Delta(2\theta)\cos\theta_0$ from XRD data, where L was the crystalline size, K was a constant (K = 0.9–1.1), λ was wavelength of X-ray (Cu Kα = 0.154 nm), and $\Delta(2\theta)$ was the width of the peak at half height.

The N_2 adsorption measurements of pore size and surface area were made at 77 K using a Quantacharome Autosorb-1 (Yuasa Ionics). Before each measurement, the sample was outgassed at 473 K for 2 h under vacuum. The specific surface area was calculated using the Brunauer–Emmett–Teller (BET) method. The pore size distribution was measured by multiple Barrett–Joyner–Halenda (BJH) methods, using adsorption branches of nitrogen adsorption–desorption isotherms.

The metal–support interaction and reduction behaviour of synthesized catalyst was characterized by temperature-programmed reduction (TPR) experiment carrying out on a catalyst analyzer BELCAT-B (BEL Japan). Typically, 30 mg catalyst was temperature-programmed reduced by a 5 vol% H_2/Ar flow (50 ml/min) from 323 K to 1073 K with a ramping rate of 10 K/min. Hydrogen consumption was monitored by TCD. Prior to each measurement, the sample was dried at 423 K for 1 h in an Ar (50 ml/min) atmosphere to remove the impurities.

High resolution transmission electron micrographs (HRTEMs) were obtained with a JEOL JEM-2100 UHR transmission electron microscope operated at 200 kV. The energy dispersive spectra (EDX) were collected by a detector that acquires signals from the selected sample area.

Nickel dispersion and nickel surface area of catalysts were determined by hydrogen chemisorption experiments (BELCAT-B, BEL Japan), assuming that one surface nickel is occupied by one hydrogen atom. The details of the hydrogen chemisorption procedure have been given elsewhere [18]. Before the H_2 chemisorption, the catalyst was reduced by 100% H_2 at 750 °C for 12 h. The Ni dispersion is determined as follows:

$$D = \frac{\text{number of } Ni^0 \text{ atoms on surface}}{\text{total number of } Ni^0 \text{ atoms}} \times 100$$

$$= \frac{\text{number of } Ni^0 \text{ atoms on surface}}{\text{total number of Ni atoms in sample}} \times 100 \text{ (fraction reduced)}$$

Coke formation was analyzed temperature-programmed oxidation (TPO) using a Shimadzu TGA/DTG-60 apparatus. The spent catalyst was temperature-programmed heated from room temperature to 850 °C at a heating rate of 10 °C/min.

3. Results and discussion

3.1. Physicochemical property of the mesoporous samples

Textural properties of support and catalysts were determined by nitrogen physical adsorption method. Fig. 1a shows the nitrogen

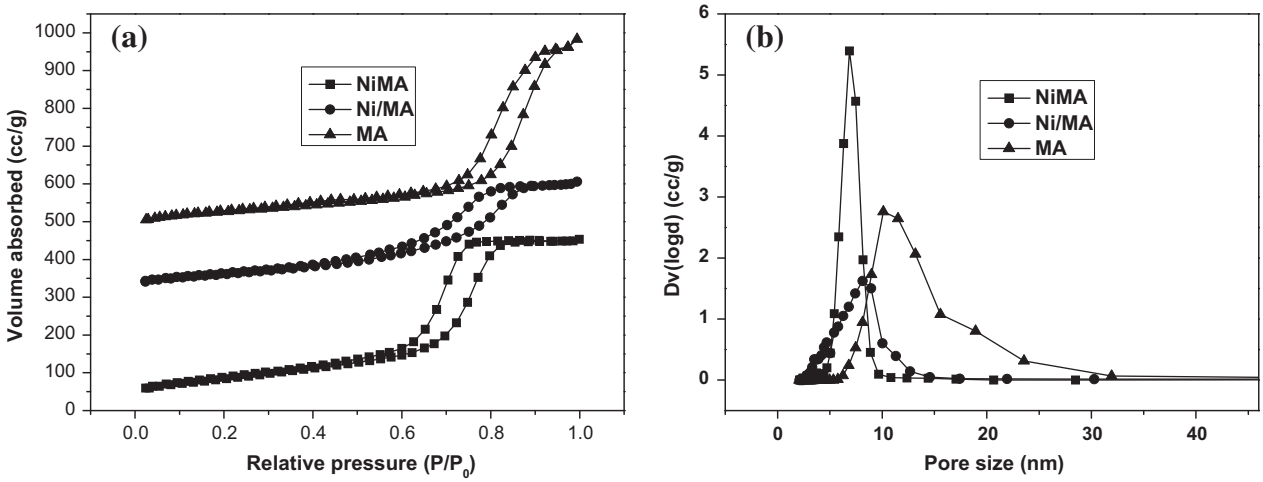

Fig. 1. Nitrogen adsorption–desorption isotherms (a) and pore size distributions (b) of NiMA, Ni/MA and MA samples calcined at 700 °C.

adsorption–desorption isotherms of MA, Ni/MA and NiMA samples. There are two kinds of hysteresis observed for all the three mesoporous samples. For MA and NiMA samples, typical IV-type isotherms with H1-type hysteresis loops were observed, which suggested the existence of well-developed cylindrical mesopores. It also should be noticed that for both NiMA and MA, the capillary condensation steps of the hysteresis loops were very steep, which suggested that the mesopore was uniformly distributed throughout the matrix of the materials. But Ni/MA catalyst prepared by impregnation method exhibited typical IV-type isotherm with H2-type hysteresis. This type of hysteresis indicated that the "bottle-neck" type pores with narrow mouths were existed. It was suggested that during the impregnation process, part of the mesoporous pore mouths was plugged by nickel species. These findings were in good accordance with previous studies [19,20]. Fig. 1b shows the BJH pore size distributions of MA, Ni/MA and NiMA samples obtained from desorption branches. All the samples retained narrow pore size distribution. Average pore size decreased in the order of MA > Ni/MA > NiMA. All the three samples consist of pores in the range of mesopore according to the curves of pore diameter distribution.

The physicochemical properties of MA, Ni/MA and NiMA were summarized in Table 1. All samples showed high surface area, large pore volume. It was observed that Ni/MA catalyst exhibited smaller average pore diameter, pore volume and lower BET surface area, compared to the mesoporous support alumina MA. Similar phenomena were also observed in previous reports [18,19]. It suggested that part of pores of mesoporous alumina were blocked by Ni species during the impregnation step and "bottle-neck" type pores were generated. This result is in good accordance to the hysteresis type mentioned above. Although the chemical composition of Ni/MA and NiMA catalysts is the same, two catalysts distinguish dramatically in the terms of BET surface area, pore volume and average pore diameter. The mesoporous nickel–alumina catalyst prepared by one-step template method exhibited superior textural properties than that prepared by impregnation method. It was inferred that nickel was homogeneously distributed in the form of Ni–O–Al composite. It also should be noted that NiMA showed larger BET surface area, lower pore volume and smaller pore diameter than MA. It was believed that some rather smaller mesopores were formed by nickel species in NiMA after calcination [21].

Table 1
Physicochemical property of samples.

Sample	MA	Ni/MA	NiMA
Surface area (m^2/g)	256.9	219.0	305.1
Pore volume (cm^3/g)	0.83	0.49	0.76
Average pore diameter (nm)	10.1	8.1	6.9

TEM images of MA, Ni/MA and NiMA were also given in Fig. 2. It was clearly observed that MA and NiMA were composed of homogeneous pores in the range of mesopore. After the introduction of nickel through impregnation, somewhat blocking of mesopores was observed in Fig. 2b; while, NiMA exhibited uniform mesoporority. The TEM result agreed well with physical adsorption result. To make a close observation of NiMA catalyst, HRTEM image is presented. As shown in Fig. 2d, atomic plane (3 1 1) with interplanar distance of 0.24 is observed, which is characteristic of the structure of $NiAl_2O_4$ [22]. The selective area electron diffraction (SAED) pattern (the insert in Fig. 2d) suggested the degree of crystallinity was low, which could also be observed in the HRTEM image. EDX measurements were also conducted by selecting a crystalline and an amorphous domain of the sample (Fig. S1 in supporting information), indicating a homogeneous distribution of Ni and Al species throughout the sample.

3.2. Crystalline analysis of catalysts and support

To understand the crystalline structure of mesoporous support and catalysts, XRD measurements were carried out. Fig. 3 presents XRD patterns of MA, Ni/MA and NiMA calcined at 700 °C for 4 h. For mesoporous alumina, there is no obvious diffraction peak observed, which indicated that the synthesized mesoporous alumina was amorphous or the Al_2O_3 crystalline size was very fine, exceeding the detection limit of XRD. For Ni/MA catalyst, there were no individual characteristic peaks of nickel oxides and alumina. Seo et al. [21] studied the XRD patterns of mesoporous alumina supported nickel catalyst calcined at 700 °C for 5 h and found that characteristic peaks of γ-Al_2O_3 shifted to low diffraction angle. The authors ascribed it to the expanding of alumina lattice caused by nickel incorporation during the high temperature treatment and nickel aluminate phase was formed. This was also observed by other authors [23]. The XRD pattern of Ni/MA catalyst of the present work is very similar to those reported [21]. It was believed that nickel aluminate ($NiAl_2O_4$, spinel) was formed through the reaction of NiO and Al_2O_3 at high temperature. The higher the calcination temperature, the larger the fraction of Ni^{2+} ions converted into spinel. At 750 °C, all of the N^{2+} ions incorporated with alumina to generate nickel aluminate phase [24,25]. In this work, Ni/MA catalyst was calcined at 700 °C for 4 h after impregnation, it was possibly

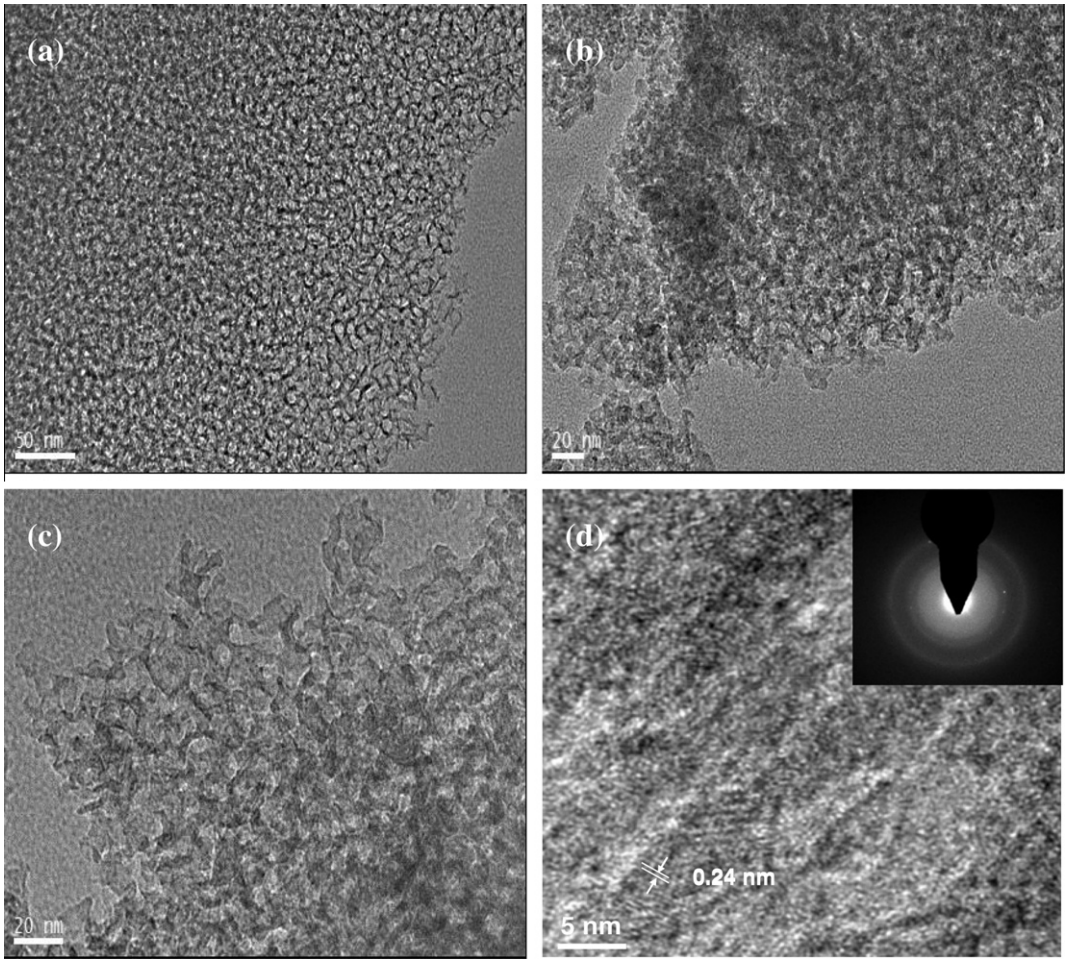

Fig. 2. TEM images of calcined MA (a), Ni/MA (b), NiMA (c), and HRTEM image of NiMA (d) (the insert in d is corresponding SAED pattern).

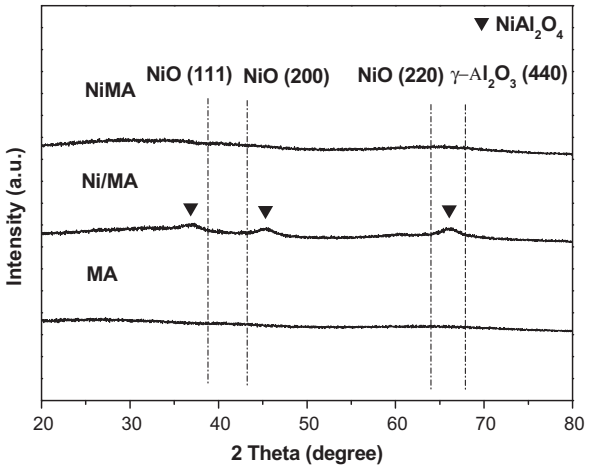

Fig. 3. XRD patterns of MA, Ni/MA and NiMA samples calcined at 700 °C for 4 h.

that a part of nickel species were strongly incorporated with alumina to form nickel aluminate phase. Although the XRD patterns for both Ni/MA and NiMA catalysts were very weak and cannot be accurately indexed, with the help of HRTEM image (Fig. 2d), SAED (inset in Fig. 2d) and EDX (Fig. S1 in supporting information), it is deduced a part of Ni and Al species formed spinel phase ($NiAl_2O_4$), while most generated amorphous Ni–Al–O species, highly dispersed throughout the catalyst. The XRD pattern of NiMA catalyst showed similar shape to that of Ni/MA, but the diffraction peaks were even broader, indicating nickel species was even finely dispersed throughout the catalyst.

3.3. Reducibility, metal–support interaction and nickel dispersion

TPR is an efficient method to characterize the reducibility of nickel supported metal catalysts. To investigate the reducibility as well as the interaction between nickel species and support in both Ni/MA and NiMA catalysts, TPR experiments were carried out. TPR profiles of Ni/MA and NiMA were given in Fig. 4. For Ni/MA or NiMA catalyst, there was only one reduction peak centred at temperature above 700 °C. It was believed that TPR profiles of supported nickel catalysts were strongly affected by the nature of metal–support interaction. The maximum reduction peak of bulk NiO free of interaction with support located at around 400 °C, depending on the preparation and method [26,27]. In our case, there was no reduction peak located in this area, suggesting the absence of isolated NiO phase, which was also in well accordance with the XRD results. The reduction peak in the high temperature region (700–827 °C) could be ascribed to the reduction of nickel species strongly interacted with alumina in the form of nickel aluminate [20,28]. Therefore, for both Ni/MA and NiMA catalysts, the reduction peak was thought to be the highly dispersed nickel aluminate and/or amorphous Ni–Al–O species, taking the HRTEM and XRD results into account. During the hydrogen reduction and the dry reforming process, the strongly interacted nickel species can be readily reduced to highly dispersed nanosized nickel particles.

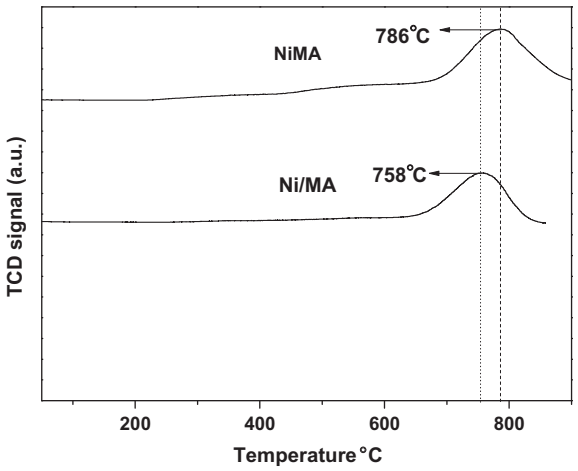

Fig. 4. TPR profiles of NiMA and Ni/MA catalysts calcined at 700 °C for 4 h.

Besides, the reduction peak of NiMA catalyst moved to high temperature zone when compared with Ni/MA, which indicated that Ni/MA catalyst was more reducible than NiMA catalyst, and the nickel–alumina interaction was stronger for NiMA catalyst.

To determine the nickel dispersion of catalysts, H_2 chemisorption measurements were carried out. Before the chemisorption measurement, the catalyst was sufficiently reduced (100% H_2 at 750 °C for 12 h), so that the reducibility is not needed for the calculation [29]. As shown in Table 2, NiMA catalyst (Ni dispersion: 19.1%, H_2 adsorption: 261.7 μmol/g) exhibited higher nickel dispersion and larger H_2 adsorption amount than that of Ni/MA (Ni dispersion: 16.9%, H_2 adsorption: 228.2 μmol/g), which revealed that nickel species were more homogeneously dispersed compared to Ni/MA, as also demonstrated by TPR result in Fig. 4.

3.4. CO_2 reforming of CH_4

Methane reforming with carbon dioxide ($CO_2 + CH_4 \rightleftarrows 2H_2 + 2CO$, $\Delta H^{\circ}_{298} = +247$ KJ mol^{-1}) is a reaction with high endothermicity, it is preferred to conduct this reaction at high temperature. Therefore, thermally stable catalyst will be beneficial to this reaction. In the present work, both NiMA and Ni/MA showed strong interaction between nickel species and support, and this interaction could retard the sintering of nickel during the thermal treatment and reaction.

Both NiMA and Ni/MA catalysts were applied for carbon dioxide reforming of methane. Fig. 5 shows CH_4, CO_2 conversion and H_2/CO ratio as a function of reaction time on stream in the methane dry reforming at 700 °C for 24 h. Both Ni/MA and NiMA catalysts showed stable catalytic performance and high activity for CO_2 reforming of CH_4. It was reported that the crystalline size of Ni had a pronounced influence in the terms of catalytic activity and stability for methane reforming, while nanosized nickel catalysts exhibited high catalytic activity and stability for carbon dioxide reforming of methane [11,30]. Highly dispersed Ni catalyst showed good coke resistance, since the ensemble size necessary for carbon formation is larger than that necessary for CH_4 dry reforming. In the present work, highly dispersed nickel aluminate was gradually reduced during the reduction and reaction process to give nanosized nickel. The formed small nickel crystalline showed good catalytic performance in the methane dry reforming. One the other hand, strong metal to support interaction (SMSI) could also prevent the coking and sintering of the nickel crystalline. Therefore, all the factors including high surface area, strong interaction between Al_2O_3 and Ni species, large pore volume and uniformly dispersed Ni species comprehensively contributed to the good catalytic performance of NiMA and Ni/MA catalysts.

Table 2
Nickel dispersion.

Catalyst	H_2 adsorption (μmol/g)	Ni dispersion (%)
NiMA	261.7	19.1
Ni/MA	228.2	16.9

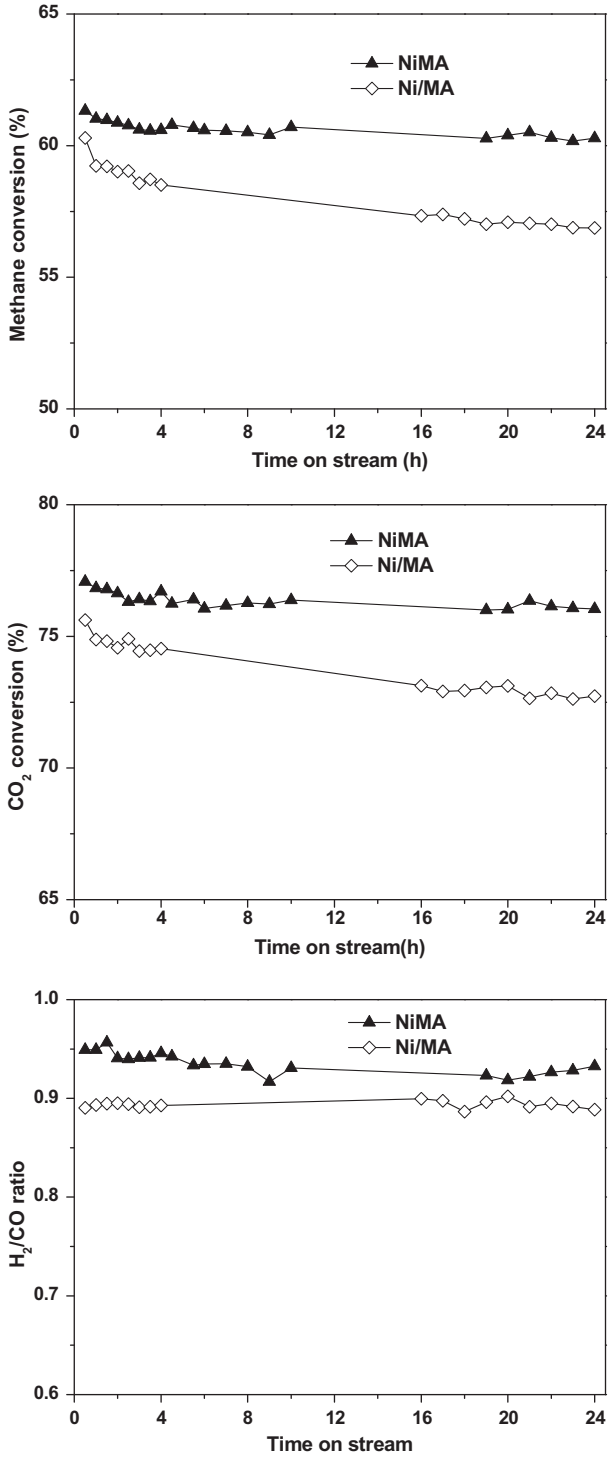

Fig. 5. Catalytic performances of NiMA and Ni/MA catalysts. Test condition: T = 700 °C, P = 0.1 Mpa, W/F = 1 g-cat h mol^{-1}.

It was noteworthy that CH_4 and CO_2 conversions of Ni/MA catalyst changed from initial 60.3% and 75.6% to 56.9% and 72.7%,

respectively, after 24 h reaction. More interestingly, no obvious decline of catalytic activity for NiMA catalyst was observed. The H_2/CO for NiMA and Ni/MA of were 0.95 and 0.89, respectively, suggesting the reverse water gas shift reaction (RWGS, $H_2 + CO_2 \rightarrow H_2O + CO$) was almost negligible. Although, there is no great improvement of catalytic activity, NiMA catalyst exhibited a superior catalytic performance to Ni/MA with more stable CH_4 and CO_2 conversions as well as H_2/CO, due to higher Ni dispersion and stronger SMSI of NiMA catalyst. The activity of NiMA can be further improved by addition of promoters [5,16].

3.5. Characterization of spent catalysts

Since coking and sintering of active metal are responsible for the catalyst deactivation, the spent catalysts here were examined by XRD measurements to characterize the coke and sintering. XRD patterns of post-reaction Ni/MA and NiMA samples are shown in Fig. 6. There were no characteristic peaks of NiO and $NiAl_2O_4$, but broad diffraction peaks of Ni were observed for both spent Ni/MA and NiMA catalysts. This suggested that the surface nickel aluminate phase was reduced completely to Ni during the high-temperature treatment and reaction, which agreed well with TPR results. The Ni crystalline sizes of both Ni/MA and NiMA catalysts were very small (<6 nm) and NiMA exhibited rather smaller Ni crystalline size, showing good thermal stability. Besides, no characteristic peaks of carbon were observed, indicating coking was negligible for the synthesized mesoporous catalysts. It was inferred that the highly dispersed nanosized nickel particles and the strong nickel–aluminate interaction could suppress nickel sintering and coking during the reaction and thus realized good catalytic performance.

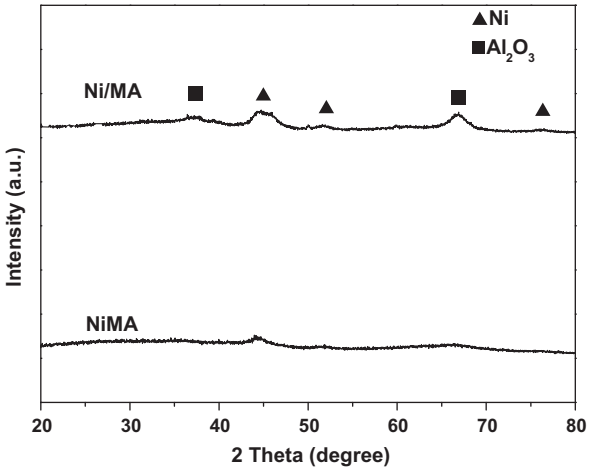

Fig. 6. XRD patterns of spent NiMA and Ni/MA catalysts.

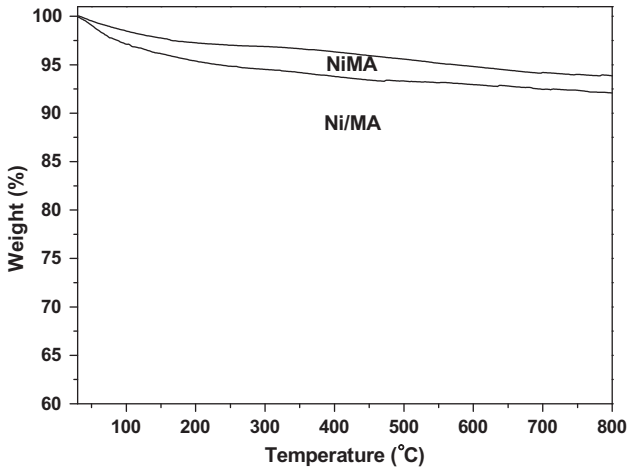

Fig. 7. TG profiles of spent NiMA and Ni/MA catalysts after 24 h reaction.

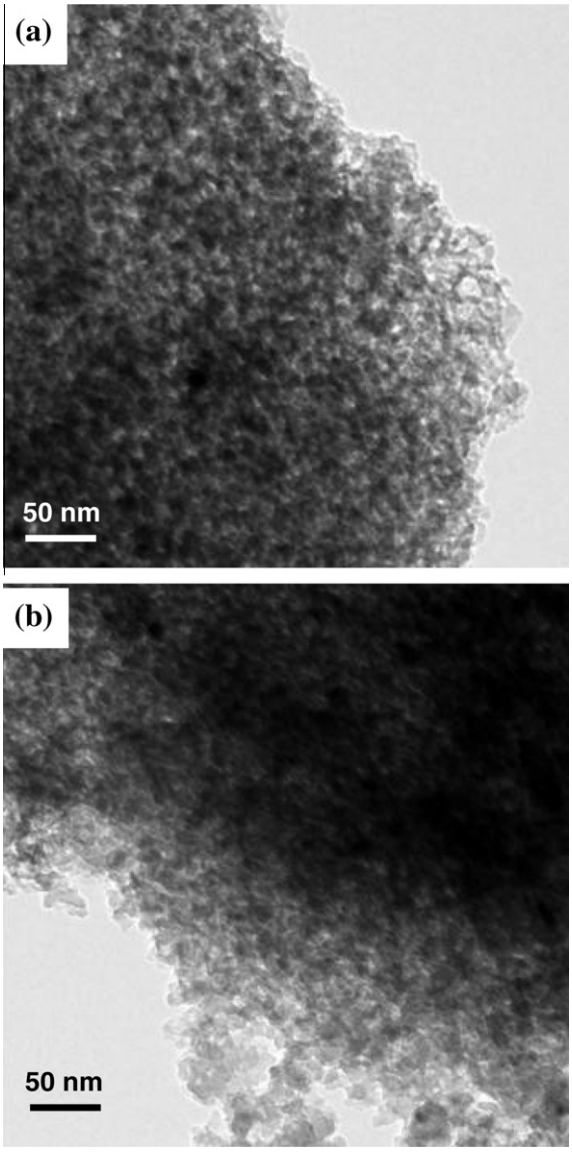

Fig. 8. TEM images of spent NiMA (a) and Ni/MA (b) catalysts after 24 h reaction.

TPO experiments were also carried out to investigate the possible coking during the reaction. For both spent Ni/MA and NiMA catalysts, there was no obvious weight losses observed, as shown in Fig. 7. It was revealed that few coke was formed, indicating that catalysts were very stable for methane dry reforming. TEM images of spent NiMA and Ni/MA catalyst was given in Fig. 8, also no formation of coke was found.

4. Conclusions

A mesoporous Ni–Al composite oxide catalyst (NiMA) prepared by a single-step surfactant-templating method and a nickel supported on mesoporous Al_2O_3 catalyst (Ni/MA) prepared by impregnation were tested in methane dry reforming. Both catalysts exhibited high BET surface area, large pore volume and narrow pore size distribution. NiMA catalyst showed superior textural properties when compared with Ni/MA catalyst. Nickels species

were well dispersed in the form of nickel aluminate and/or amorphous Ni–Al–O species for both catalysts. During the reduction and reaction, nickel species was gradually reduced to generate highly dispersed nanosized nickel particles. Both catalysts showed good catalytic performance in methane dry reforming, due to the small nickel crystalline and strong metal to support interaction, since highly dispersed nickel species could suppress coking and strong SMSI could resist sintering. However, NiMA catalyst exhibited better catalytic performance than Ni/MA catalyst. This can be explained by higher nickel dispersion and stronger nickel–alumina interaction for NiMA than those for Ni/MA. Hence, NiMA catalyst prepared by one step template method could be served as a superior catalyst candidate for carbon dioxide reforming of methane.

Acknowledgments

The authors are grateful for the financial support from the National Science Foundation of China (Grant Nos. 51072204 and 51172249), and the Natural Science Foundation of Zhejiang Province (Grant No. Y4100695) and the Ministry of Science and Technology of China (Grant No. 2012DFA40550).

Appendix A. Supplementary material

Supplementary data associated with this article can be found, in the online version, at http://dx.doi.org/10.1016/j.cej.2013.01.073.

References

[1] J.-Y. Cheon, S.-H. Kang, J.W. Bae, S.-J. Park, K.-W. Jun, G. Murali Dhar, K.-Y. Lee, Catal. Lett. 134 (2009) 233.
[2] J. Zhu, X. Peng, L. Yao, J. Shen, D. Tong, C. Hu, Int. J. Hydrogen Energy 36 (2011) 7094.
[3] R. Wang, H. Xu, X. Liu, Q. Ge, W. Li, Appl. Catal. A 305 (2006) 204.
[4] B. Nematollahi, M. Rezaei, M. Khajenoori, Int. J. Hydrogen Energy 36 (2011) 2969.
[5] K. Tao, Y. Zhang, S. Terao, N. Tsubaki, Catal. Today 153 (2010) 150.
[6] K. Tao, Y. Zhang, S. Terao, Y. Yoneyama, T. Kawabata, K. Matsuda, S. Ikeno, N. Tsubaki, Chem. Eng. J. 170 (2011) 258.
[7] S. Damyanova, B. Pawelec, K. Arishtirova, J.L.G. Fierro, Int. J. Hydrogen Energy 36 (2011) 10635.
[8] F. Pompeo, N.N. Nichio, O.A. Ferretti, D. Resasco, Int. J. Hydrogen Energy 30 (2005) 1399.
[9] K.Y. Koo, H.-S. Roh, Y.T. Seo, D.J. Seo, W.L. Yoon, S. Bin Park, Int. J. Hydrogen Energy 33 (2008) 2036.
[10] M.C.J. Bradford, M.A. Vannice, Catal. Rev. Sci. Eng. 41 (1999) 1.
[11] I. Črnivec, P. Djinović, B. Erjavec, A. Pintar, Chem. Eng. J. 207–208 (2012) 299.
[12] S. Zhang, J. Wang, H. Liu, X. Wang, Catal. Commun. 9 (2008) 995.
[13] T. Wang, J. Chang, X. Cui, Q. Zhang, Y. Fu, Fuel Process. Technol. 87 (2006) 421.
[14] Y. Cui, H. Zhang, H. Xu, W. Li, Appl. Catal. A 331 (2007) 60.
[15] X. Yu, N. Wang, W. Chu, M. Liu, Chem. Eng. J. 209 (2012) 623.
[16] N. Wang, W. Chu, T. Zhang, X. Zhao, Chem. Eng. J. 170 (2011) 457.
[17] S.M. Morris, P.F. Fulvio, M. Jaroniec, J. Am. Chem. Soc. 130 (2008) 15210.
[18] J.G. Seo, M.H. Youn, I.K. Song, Int. J. Hydrogen Energy 34 (2009) 1809.
[19] J. Horiguchi, Y. Kobayashi, S. Kobayashi, Y. Yamazaki, K. Omata, D. Nagao, M. Konno, M. Yamada, Appl. Catal. A 392 (2011) 86.
[20] L. Xu, H. Song, L. Chou, Catal. Sci. Technol. 1 (2011) 1032.
[21] J. Seo, M. Youn, D. Park, J. Jung, I. Song, Catal. Lett. 132 (2009) 395.
[22] Y. Liu, S. Wang, T. Sun, D. Gao, C. Zhang, S. Wang, Appl. Catal. B 119–120 (2012) 321.
[23] Z. Hou, T. Yashima, Appl. Catal. A 261 (2004) 205.
[24] R. Yang, C. Xing, C. Lv, L. Shi, N. Tsubaki, Appl. Catal. A 385 (2010) 92.
[25] J.M. Rynkowski, T. Paryjczak, M. Lenik, Appl. Catal. A 106 (1993) 73.
[26] Z. Hou, O. Yokota, T. Tanaka, T. Yashima, Appl. Catal. A 253 (2003) 381.
[27] J. Juanjuan, M. Romanmartinez, M. Illangomez, Appl. Catal. A 301 (2006) 9.
[28] J.I. Villacampa, C. Royo, E. Romeo, J.A. Montoya, P. Del Angel, A. Monzón, Appl. Catal. A 252 (2003) 363.
[29] H. Xiong, Y. Zhang, K. Liew, J. Li, J. Mol. Catal. A 231 (2005) 15.
[30] Q.-H. Zhang, Y. Li, B.-Q. Xu, Catal. Today 98 (2004) 601.